Metal Organic Polyhedron with Four Fe(III) Centers Producing Enhanced T_1 MRI Contrast in Tumors

Gregory E. Sokolow,[1] Matthew R. Crawley,[1] Daniel R. Morphet,[1] Didar Asik,[1] Joseph A. Spernyak,[2] A. J. Robert McGray,[3] Timothy R. Cook,[1*] and Janet R. Morrow[1*]

[1] Department of Chemistry, University at Buffalo the State University of New York, Buffalo, NY 14260.
[2] Department of Cell Stress Biology, Roswell Park Comprehensive Cancer Center, Buffalo, NY 14263.
[3] Department of Immunology, Roswell Park Comprehensive Cancer Center, Buffalo, NY 14263.

KEYWORDS iron coordination complexes, metal organic polyhedron, magnetic resonance imaging

ABSTRACT: A metal organic polyhedron (MOP) with four paramagnetic Fe(III) centers was studied as a magnetic resonance imaging (MRI) probe. The MOP was characterized in solution by using EPR and UV-vis spectroscopies, FT-ICR mass spectrometry, and in the solid state with single crystal x-ray diffraction. Water proton T_1 relaxation properties were examined in solution and showed significant enhancement in the presence of human serum albumin (HSA). The r_1 relaxivities in the absence and presence of HSA were 8.7 $mM^{-1}s^{-1}$ and 21 $mM^{-1}s^{-1}$, respectively, per molecule (2.2 and 5.3 per Fe) at 4.7 T, 37 °C. In vivo studies of the iron MOP show strong contrast enhancement of blood pool even at a low dose of 0.025 mmol/kg with prolonged residence in vasculature and clearance through the intestinal tract of mice. The MOP binds strongly to serum albumin and shows comparable accumulation in a murine tumor model as a covalently linked Gd-HSA contrast agent.

INTRODUCTION

Gd(III) coordination complexes have been successfully developed as contrast agents for clinical magnetic resonance imaging (MRI) procedures.[1-3] Control over the bio-distribution of the Gd(III) complexes is accomplished by modulating charge and lipophilicity through incorporation of functional groups on ligand structures.[4-7] This approach has produced contrast agents that are utilized in nearly 40% of clinical MRI procedures.[8] Gd(III) complexes were originally examined because of their favorable proton relaxation properties. Gd(III) has seven unpaired electrons (S = 7/2) with slow electronic relaxation attributed to a symmetric S electronic ground state. In addition, the coordination sphere of Gd(III) can accommodate multiple exchangeable water ligands with exchange rates (k_{ex} =10^6-10^8 s^{-1}) that are favorable for enhancement of T_1 water proton relaxivity at magnetic field strengths used in clinical MRI.[7] However, concerns of gadolinium deposition and nephrogenic systemic fibrosis[9-14] from these MRI contrast agents has sparked a resurgence in the development of alternative contrast media which rely on transition metals in place of Gd(III).

The corresponding shift in focus towards high-spin Fe(III) and Mn(II) metal centers has created a need for new ligand scaffolds that are better suited to stabilize these paramagnetic centers.[15-17] Both high-spin Fe(III) and Mn(II) have five unpaired electrons (S = 5/2) and are potentially suitable replacements for Gd(III) in terms of electronic relaxation rates. However, whereas the preparation of Mn(II) contrast agents with exchangeable water ligands is feasible, the smaller ionic size of Fe(III) and correspondingly large Lewis acidity makes it more difficult to design contrast agents which rely on water ligand exchange to increase relaxation rates, especially for 6-coordinate Fe(III). Analogous to Gd(III) agents, transition metal contrast agents may enhance proton relaxivity through several distinct mechanisms including exchange of inner-sphere water, second-sphere or outer-sphere water or by exchange of ligand protons.[18]

Fe(III) coordination complexes utilizing polyaminocarboxylate scaffolds, EDTA and DTPA have been reported as MRI contrast agents but, despite an exchangeable inner-sphere water, the Fe(III) complexes demonstrated lower r_1 relaxivity than their Gd(III) counterparts in solution and were used at higher concentrations in vivo.[19] More recent examples of Fe(III) complexes with diaminocyclohexyl backbone and a combination of carboxylate and heterocyclic donors show enhanced relaxivity in solution.[19-21] Interestingly, the latter class of complexes undergoes dimerization upon deprotonation of bound water ligands which has been proposed as a means to track pH.[22] Macrocyclic chelates of triazacyclononane with alcohol pendants have been tailored towards the smaller Fe(III) ion.[23-25] These complexes have well-defined solution chemistry and MRI studies of mice revealed promising T_1-weighted enhancements complemented by kidney specific localization. It is also remarkable that the contrast enhancement for these complexes is large despite lacking readily exchangeable water ligands and reliance

on second-sphere water exchange. A very recent example of a bis-chelated Fe(III) center that lacks bound water shows that this approach can be extended to additional types of ligands.[26]

Early studies of Fe(III) contrast agents that mediate proton relaxation through second-sphere water interactions include Fe(III)-catechol complexes as reported by Davis in 1996.[27] The tris-catecholate structures of iron are fully coordinated by the catechol donors, preventing binding of water to give inner-sphere water ligands. Despite promising initial results, further exploration of these complexes has not been pursued aside from recent reports on bimodal catechol iron agents.[28-29] One requisite for the further development of these complexes as MRI contrast agents is the need to increase their stability and kinetic inertness towards loss of a catechol ligand. Another is to increase the overall relaxivity as has been reported for related tannic acid derivates that form nanoparticles.[28, 30-31] Considering this research, we were inspired to create well-defined multinuclear Fe(III) centers by linking catechol moieties.

Proton water relaxation rates in the presence of multinuclear Fe(III) centers are expected to be influenced by correlations times describing the following; the lifetimes of resonating nuclei, τ_m, electronic relaxation of the metal center, τ_s, and by induced fluctuations of the localized magnetic field at a nucleus due to correlated rotational motion of unpaired electrons and protons, attributed to τ_r. For Fe(III) complexes that lack an inner-sphere water, the limiting correlation times are associated with rotational motion and electronic relaxation.[32] The synthesis of high-molecular-weight polymers which increase relaxivity by slowing molecular rotation and by incorporating multiple paramagnetic ions has been reported for Gd(III) agents, but fast localized motions in polymer systems produce enhancements that were less than expected.[33-34] Systems with multiple paramagnetic centers rigidly linked are more successful in producing high relaxivity agents.[35-36] In this vein, dinuclear Fe(III) complexes are effective MRI probes, although relaxivity is only slightly larger than additive for the two iron centers.[25, 37] Finally, the contribution of the electronic relaxation time of Fe(III) complexes based on their coordination sphere and zero-field splitting (ZFS) parameters has been analyzed and it is clear that further research in this area is needed.[32]

In order to create rigidly linked Fe(III) centers, we noted that self-assembled metal organic polyhedra (MOPs) containing catechol donors could be used for MRI applications through the development of iron templated gadolinium-based triple helicate complexes.[38-40] These complexes display promising contrast enhancement attributed to the coordinated Gd(III) lanthanide centers that can accommodate exchangeable inner-sphere waters. Additionally, Raymond and coworkers developed a variety of self-assembled architectures utilizing Ga(III) and Fe(III) catecholate linkers producing a variety of MOP geometries, but focused on proton relaxation properties of the Gd(III) centers. Following similar principles for self-assembly, but with a focus on the relaxation properties of Fe(III), we prepared polyhedral MOPs based these principles[41] which also piqued the interest of the Yang Group.[42]

Herein we report the use of rigid catecholamide linkers for a M_4L_6 MOP utilizing multiple Fe(III) centers in a high molecular weight rigid structure which shows increased relaxivity compared to Fe(III) catecholates and closed coordinate macrocyclic complexes. Notably, this self-assembly is kinetically inert in the presence of Zn(II) cations and EDTA for up to 24 hours, in contrast to simple catechol complexes of Fe(III) which rapidly decompose under such conditions. Effective proton relaxation effects are observed despite the closed-coordinate Fe(III) centers. The strong protein interactions observed in-vitro and in binding studies reflect the in-vivo pharmacokinetic properties observed in mouse models and in the dramatic increases observed with T_1 relaxivity in the presence of human serum albumin (HSA).

RESULTS AND DISCUSSION

The ligand H_4A was chosen based on the M(III), M(IV) tetrahedral cages developed by Raymond and coworkers.[43-45] The ligand was synthesized following a general procedure (Scheme S1) adapted from the literature. Rigidity in the catecholamide ligand is important to form discrete MOPs as it prevents the ligand from chelating the same metal center with both catechol donors. Additionally, the increased rigidity helps minimize localized molecular motions which may reduce relaxation enhancement as observed in polymer and metallo-star based contrast agents.[46-47]

The MOPs were synthesized with careful stochiometric control in methanol using six equivalents of ligand to four equivalents of trivalent metal salts. The Fe(III) reaction mixtures changed from a green to blue to deep red with increasing additions of KOH indicative of the formation of tris-catecholate Fe(III) centers. Ga(III) reaction mixtures turned yellow under similar treatment with KOH.

The ^{1}H NMR spectra of Fe(III) high-spin complexes suffer from line broadening due to effective proton relaxation as seen for Fe_4A_6 (Figure S8). Magnetic moments as measured by Evans method[48] for the iron complex gives a μ_{eff} of 5.9 (Figure S11) normalized to the iron concentration. Ga(III) MOPs were prepared as a diamagnetic analog for corresponding Fe(III) high-spin species due to similar ionic radii (6 coordinate), 0.62 Å and 0.65 Å respectively resulting in similar self-assembled structures with useful ^{1}H NMR spectra (Figure S9).

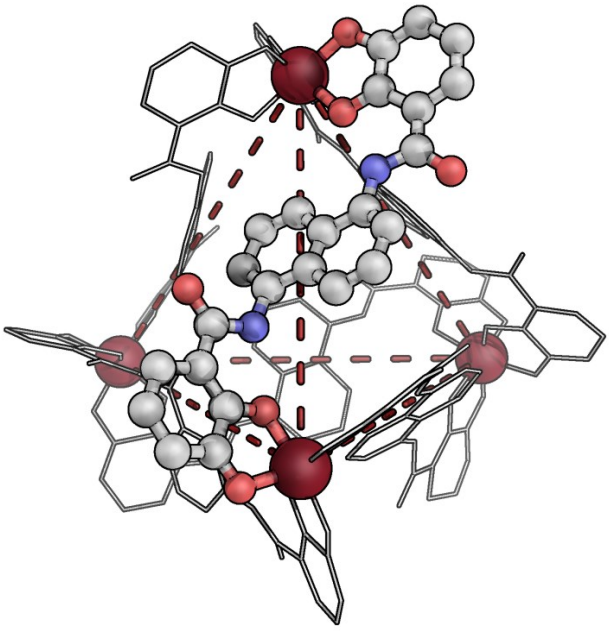

Figure 1. SC-XRD model of Fe_4A_6 superimposed over a tetrahedron (dashed red). H-atoms, counter-ions and solvent removed for clairity.

The diamagnetic analog Ga_4A_6 can be used to estimate the hydrodynamic diameter of the iron assembly by determining the diffusion coefficient from diffusion ordered spectroscopy NMR (Figure S10) and the Stokes-Einstein equation.[49-50] The hydrodynamic diameter of Ga_4A_6 in aqueous solution was determined to be 3.3 nm which is in good agreement with the crystal structure of the iron self-assembly (~2 nm).

Crystals of $K_8(NEt_4)_4[Fe_4A_6]$ were grown by vapor diffusion of diethyl ether into a methanol water solution containing the Fe(III) MOP in a similar fashion as reported by Raymond.[45] The twist angles of the Fe(III) catecholate centers were calculated to be 44.3 ° and 56.7 ° (Figure S12) for the MOP Fe_4A_6. The deviation from 60° in a perfect octahedral environment shows that the coordination geometry around the metal centers are in a distorted octahedral conformation. Higher order symmetry for a paramagnetic center can result in smaller zero field splitting effects which can slow the relaxation of electronic states manifesting in longer τ_s values.[51]

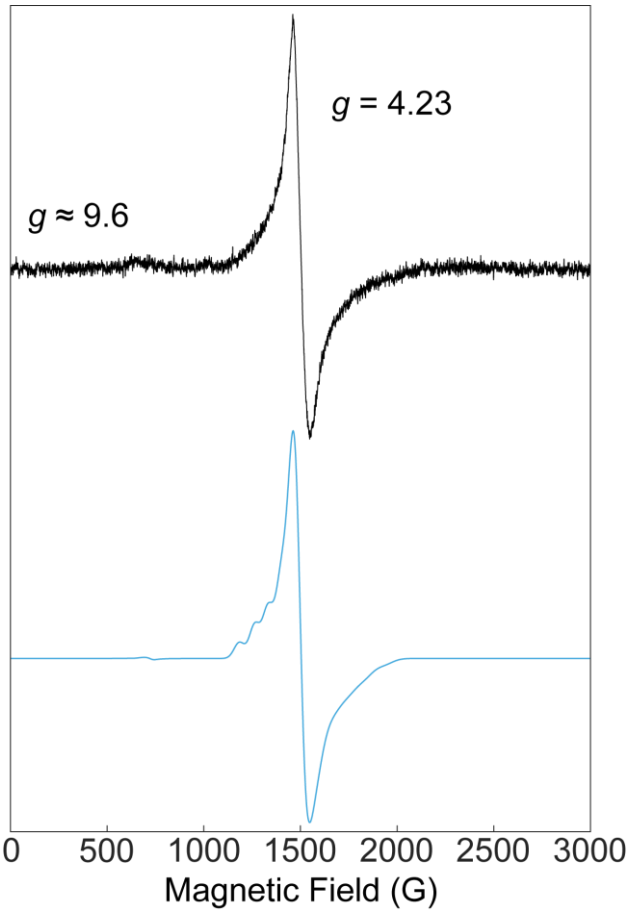

Figure 2. EPR spectrum (Black) of Fe_4A_6 at 77 K in a frozen glass (1:1 methanol and toluene). Prominent feature at $g \approx 4.23$ is consistent with a transition within the ±3/2 Kramer's doublet. Simulated spectrum (Blue) of Fe_4A_6. The principle values of the *g*-tensor were found to be: g = 4.238, 3.654, 4.7462, the principle values of the *A*-tensor: A = [21.9, 286, 17.1] MHz, g-strain = 0.21 mT, and an *E/D* ratio of 0.27, and a Gaussian line broadening of 1.28 mT.

EPR spectroscopy was used for further characterization of the Fe(III) MOP. The observable transitions originating from Kramer's doublets at g = 4.23 and a weak transition at g ≈ 9.6 are characteristic of a Fe(III) high-spin center in a tris-catecholate environment. This also suggests that the Fe(III) catecholate centers of the Fe_4A_6 are electronically isolated from one another with no communication between the paramagnetic centers. Furthermore, the lack of additional splitting of the feature at g = 4.23 suggest that there is no significant contribution from a Fe(III) bis-catecholate impurity as seen in simple mononuclear catecholate systems.[52-56] The simulated spectrum of Fe_4A_6 predicted principal values of the g-tensors to be g = 4.238, 3.654, 4.7462 and is consistent with a rhombic system. This was found to be in good agreement with the calculated ratio of the Zero-field splitting parameters E and D calculated to be 0.27 close to the theoretical limit of E/D = 1/3 for an idealized rhombic system.

The electronic absorbance spectra of the Fe(III) MOP showed a characteristic ligand to metal charge transfer (LMCT) band with an extinction coefficient of 15,100 M^{-1} cm^{-1} or 3780 M^{-1} cm^{-1} per iron centered at 514 nm.[42] This is similar to that observed with tris-catecholate iron(III) complexes. However, it should be noted that unlike the Fe_4A_6 MOP, the tris-catecholate iron(III) complex is not stable at pH 7.4, favoring a bis-chelate structure displayed by a characteristic shift in the LMCT band with pH (Figure S24). It is likely that a macro-chelate effect of the cage helps stabilize the Fe_4A_6 MOP towards pH changes. The onset of catecholate protonation occurs at a lower pH than the monomeric counterpart (Figure S23) further stabilized by polydentate ligands coordinating multiple metal centers. The LMCT band was useful to determine the inertness of the MOP towards metal dissociation. The MOP showed marked inertness in solutions of over 100-fold excess phosphate anions with no measurable change over 720 minutes at a pH of 7.4 and a temperature of 37 °C (Figure S19). Similar results were obtained under cationic stress, with nearly 40-fold excess $Zn(NO_3)_3$ over the same timeframe at 37 °C and pH of 7.4 adjusted with 20 mM HEPEs buffer (Figure S21) or in the presence of excess EDTA (Figure S22).

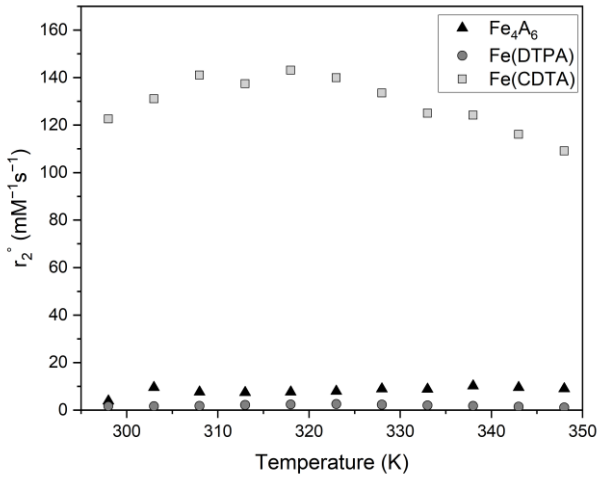

Figure 3. ^{17}O NMR transverse relaxivity ($r_2°$) for Fe(CDTA) at pH 6.8, Fe(DTPA) at pH 6.8, and Fe_4A_6 at pH 7.4 as a function of temperature.

Variable-temperature ^{17}O NMR spectroscopy experiments have been used to probe the coordination environment of paramagnetic complexes of Fe(III), Fe(II), Mn(II) and Co(II).[25, 57-58] The $^{17}OH_2$ transverse relaxation rate constants, as estimated by the linewidth, are influenced by the concentration of the paramagnetic center, the number of accessible coordination sites (q), and the residency time of the $^{17}OH_2$.[58] It should be noted that if the residency time of the interacting $^{17}OH_2$ is sufficiently long it will not contribute to observable line broadening effects. The transverse relaxation effects on $^{17}OH_2$ have been studied for

complexes like Fe(CDTA) which have an exchangeable water ligand (q = 1) and Fe(DTPA) which has no bound waters (q = 0). When normalized to Fe(III) concentration and compared to Fe(CDTA) and Fe(DTPA), Fe_4A_6 has comparable line broadening to Fe(DTPA). This suggests that the Fe(III) MOP maintains a closed coordination sphere in solution, which is inaccessible to inner-sphere water ligands. Additionally, samples prepared with human serum albumin (HSA) displayed no significant difference in line broadening of the $^{17}OH_2$ resonance and LMCT band suggesting that the coordination environment remains intact (Figure S14 and Figure S20). Thus, inner-sphere relaxation mechanisms do not contribute to the observed relaxivity associated with Fe_4A_6.

The r_1 relaxivities for the MOP were determined using inversion recovery experiments conducted on 1.4 T and 4.7 T instruments. Fe_4A_6 showed excellent proton relaxivity at both magnetic field strengths, 8.3 (1.4 T, 33 °C) and 8.7 $mM^{-1}s^{-1}$ (4.7 T, 37 °C). When normalized for iron content, the relaxivity of Fe_4A_6 is comparable to macrocyclic counterparts in Fe(TOB) and Ga(DOTA) as shown in Table 1. These data for the MOP are about 30% higher than a previous report, but the authors of that report did not specify temperature, or pH and were recorded at a lower field strength of 1 T.[42] Additionally, the previous study determined a hydrodynamic diameter of 105 nm[42] for the iron MOP utilizing dynamic light scattering which two orders of magnitude larger than the that determined by DOSY NMR studies here which could indicate a difference in complex speciation or the presence of iron oxides.

Samples prepared with 35 mg/mL human serum albumin (HSA) displayed marked increases in relaxivity of 26 and 21 $mM^{-1}s^{-1}$ at 1.4 and 4.7 T respectively. The increase in relaxivity is likely a result of a dramatic increase in the rotational correlation time of the contrast agent in solution upon binding the large globular protein (~66500 Da). Similar increases in relaxivity were observed for complexes such as MS-325 which specifically target HSA.[4-6, 59] Binding of Fe_4A_6 to HSA was further investigated using an ultrafiltration method to gauge binding strength. In this method, the HSA bound Fe(III) complex is separated from the free complex by ultrafiltration and the iron content of the filtrate is determined by using ICP-MS. Binding isotherms (Figure S19 and Figure S20) are consistent with a strong interaction ($K_a \approx 10^5$ M^{-1}) of the Fe(III) MOP with HSA and the shape of the isotherm is consistent with binding of multiple MOPs to a single HSA.

To better study stoichiometry of binding, a series of titrations were carried out. One titration has excess HSA with fixed contrast agent concentration (Figure 4A) and one has fixed HSA and variable contrast agent concentration (Figure 4B).[60] The change in slope of Figure 4A at a 5:1 ratio of Fe_4A_6 to HSA is

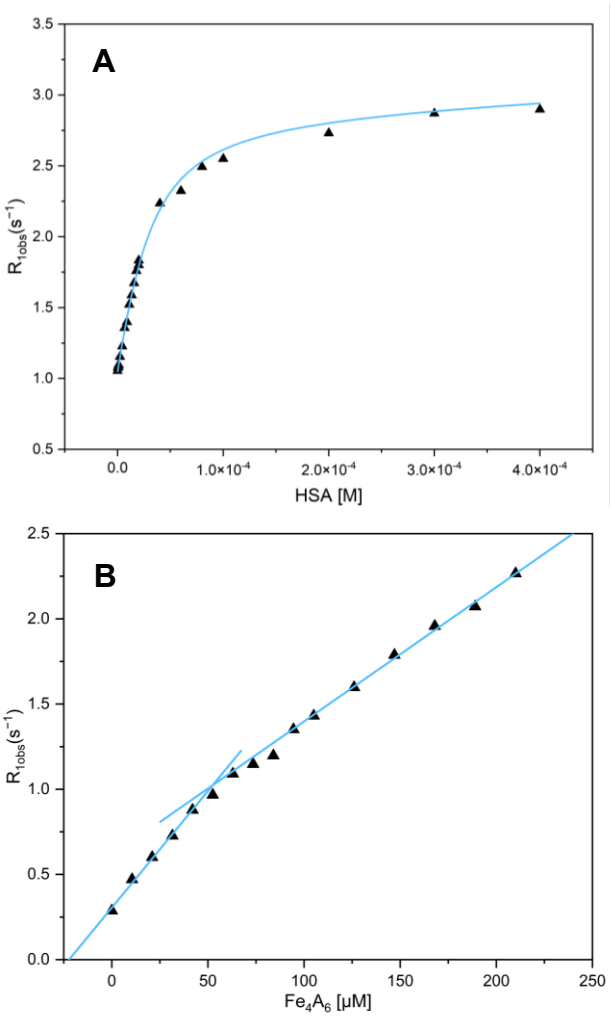

Figure 4. (A) Observed relaxation rate constants as a function of HSA concentration for a solution of 110 μM Fe_4A_6 at pH 7.4 in 1x PBS. Data was fit to equation S3 with fit parameters provided in Table S2. (B) Observed relaxation rate as a function of Fe_4A_6 concentration for a solution of 10 μM HSA in 1x PBS. Linear fits provided in supplemental in Table S3 and Table S4.

consistent with the non-competitive and non-cooperative binding of five of the Fe-MOPs to HSA, all with similar binding constants, K_a. The average value of the five K_a was determined to be 1.2×10^4 M^{-1} utilizing the changes in the observed relaxation rate and a Levenberg Marquardt fitting algorithm.[26] However, the high micromolar amounts of cage and albumin used in these studies limits our determination of binding constants that are much greater than 10^4. The determination of an average binding constant is our best approximation to fit data in hand

Table 1. Water proton r_1 relativity values for Fe(III) and Gd(III) complexes normalized to complex concentration with and without HSA.

Complex	r_1 (mM^{-1} s^{-1}) 1.4 T	r_1 (mM^{-1} s^{-1}) 4.7 T	r_1 (mM^{-1} s^{-1}) with HSA 1.4 T	r_1 (mM^{-1} s^{-1}) with HSA 4.7 T
Fe_4A_6	8.3 ± 0.3 (2.1 ± 0.1*)	8.7 ± 0.2 (2.2 ± 0.1*)	26 ± 0.1 (6.5 ± 0.1*)	21 ± 0.3 (5.2 ± 0.1*)
Fe(TOB)[b]	-	2.2 ± 0.3	-	2.5 ± 0.1
Gd(DOTA)	3.3 ± 0.5[c]	2.7-2.9[d]	-	-
Gd(DTPA)[c]	4.2 ± 0.1	3.1 ± 0.3	-	3.2 ± 0.3

*Relaxivity values for Fe_4A_6 were prepared in 1x PBS pH 7.4. *Relaxivity values reported per Fe. Relaxivity values for Fe(TOB) (define) were previously reported in 100 mM HEPES buffer pH 7.2. Gd(III) complexes contained meglamine excipient and were reported previously. Measurements at 1.4 T and 4.7 T were at 33 °C and 37 °C respectively. [b]From ref 22. [c]From ref 24. [d]From ref 23.*

and is likely more complicated.[1] The titration in Figure 4B is also consistent with a 5:1 iron MOP to HSA binding interaction. The gradual sloping line above this break suggests that there may be additional weaker binding of additional molecules of Fe_4A_6 to HSA which may be convoluted from paramagnetic contributions from free Fe_4A_6.

The strong binding of the Fe(III) MOP to serum albumin and its high relaxivity for the bound complex (r_1 of 21 $mM^{-1}s^{-1}$ at 4.7 T) suggests that the MOP will remain bound to serum albumin in animals and not extravasate into the tissue. Thus, the complex will selectively enhance the vasculature as an example of a blood pool agent. T_1-weighted maximum intensity projections given in Figure S24 at 45 minutes post injection indeed show significant signal enhancements in the vasculature of BALB/c mice. An increase in the change in proton relaxation with increasing doses of Fe_4A_6 was observed in the blood and liver for intravenous injections of Fe_4A_6 (12.5, 25 and 50 µmol/kg).

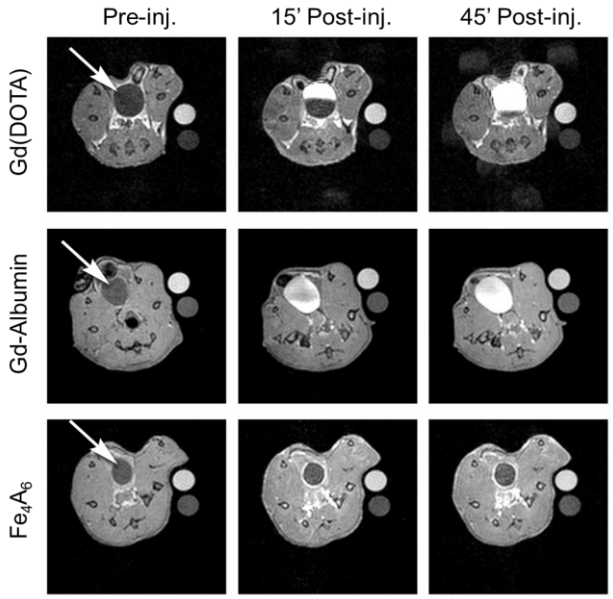

Figure 5. Representative MR images of urinary bladder before (left), 15 minutes (center) and 45 minutes (right) administration of contrast agents. Signal enhancement was observed within the bladder for Gd-DOTA (top) and Gd-Albumin (center), while little to no signal enhancement was observed for Fe_4A_6 (bottom) as far out as 4 and 24 hours (not shown).

Clearance of Fe_4A_6 occurs predominantly through the hepatobiliary system, as shown by increased signal intensity in the intestines at four hours post-injection (Figure 5 and Figure S25). This differs significantly from the clearance of MS-325, a gadolinium-based blood pool contrast which exhibits reversible binding to HSA and is excreted through the renal system.[5] Fe_4A_6 was further investigated in vivo using BALB/c mice with subcutaneous ovarian tumors and compared to a Gd(III)-Albumin contrast agent as well as a conventional Gd contrast agent, Gd(DOTA). T_1-weighted signal changes were tracked over a 4-hour period with additional measurements taken at 24-hours post injection (Figure 6). Fe_4A_6 behaved in a similar fashion to the covalently tethered Gd(III) contrast, Gd-Albumin.[61] Both Fe_4A_6 and Gd-Albumin had greatly increased retention times in the vasculature, clearing completely after 24-hours as compared to Gd(DOTA) which cleared under 4-hours. The similarities in tissue localization for the two contrast agents suggest that albumin proteins dictate their bio-distributions and slow their clearance rates. Significant signal enhancement observed in the intestinal tract after 4 hours in conjunction with enhancements in the gall bladder and liver also supports Fe_4A_6 clearance through a hepatobiliary mechanism. Unlike Gd(DOTA) and macrocyclic contrast agents.[23-25] Fe_4A_6 produced minimal changes in signal intensity in the bladder over the course of 24 hours. This is likely a result of strong albumin binding as it is well established that renal clearance of HSA is minimal with additional internalization in the proximal tubules of nephrons minimizing accumulation in the bladder.[62]

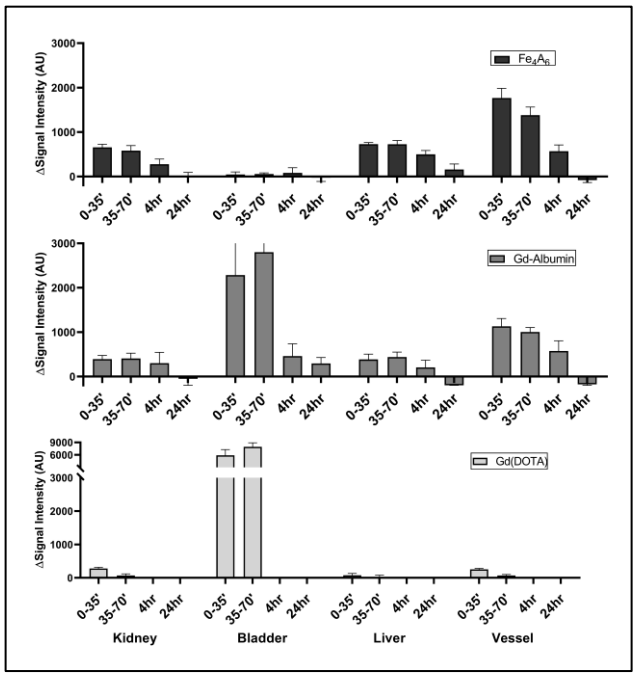

Figure 6. Changes in T_1-weighted signal intensity observed in mice for Fe_4A_6 at 12.5 µmol/kg (dark gray), Gd-Albumin at 25 µmol/kg (gray), and Gd(DOTA) 50 µmol/kg (light gray). Dosing normalized to give similar signal enhancements in-vitro. Signal changes were averaged for the time points 0-35 minutes, 35-70 minutes, 4 hours, and 24 hours apart from Gd(DOTA), which was limited to under 4 hours as a result of faster clearance rates.

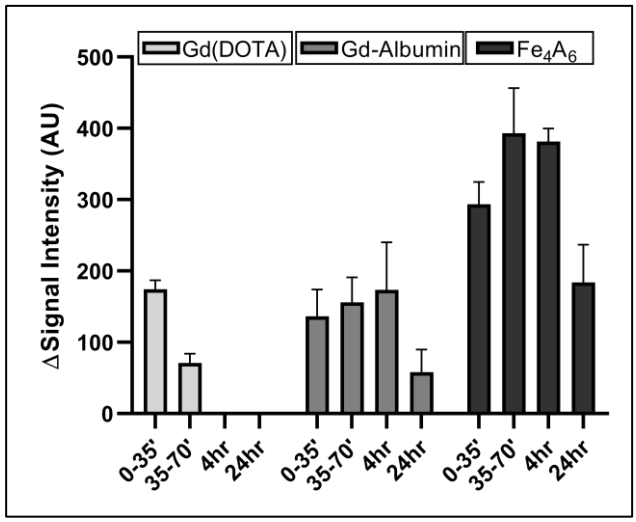

Figure 7. Changes in T_1-weighted signal intensity observed in subcutaneous ovarian tumors for Fe_4A_6 at 12.5 µmol/kg (dark gray), Gd-Albumin at 25 µmol/kg (gray), and Gd(DOTA) 50 µmol/kg (light gray). Signal changes were averaged for the time points 0-35 minutes, 35-70 minutes, 4 hours, and 24 hours apart from Gd(DOTA), which was limited to under 4 hours as a result of faster clearance rates

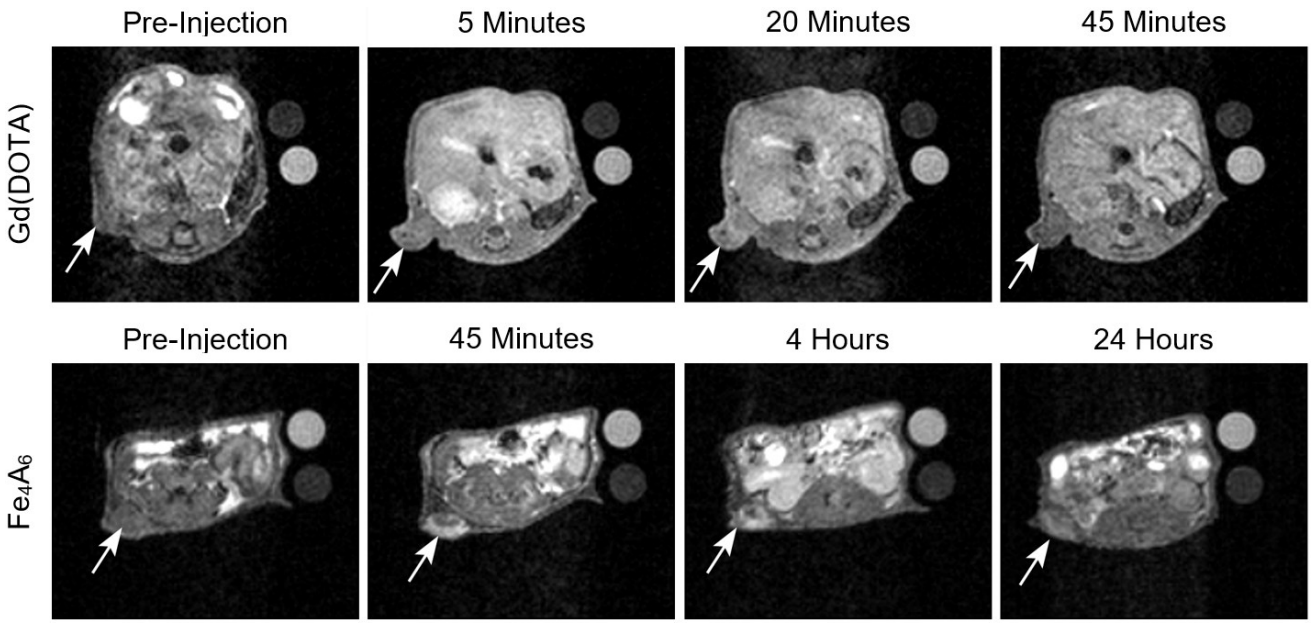

Figure 8. Example images of signal enhancement of subcutaneous ID8 ovarian cancer tumors (arrow). Top row: Gd(DOTA) at 50 μmol/kg pre-injection, 5 minutes, 20 minutes, and 45 minutes post-injection. Bottom row: Fe_4A_6 at 12.5 μmol/kg pre-injection, 45 minutes, 4 hours, and 24 hours post-injection. To improve image clarity, three or four MR scans centered around nominal time points were averaged.

Fe_4A_6 displayed promising tumor imaging properties. Signal enhancements in subcutaneous ovarian tumors increased post-injection with a peak contrast enhancement at 4 hours denoted by the contrast to noise ratio (CNR) of tumor to skeletal muscle in Figure S26. Additionally, signal enhancement in tumors was observed 24 hours post-injection (Figure 7 and Figure 8) despite the contrast agent clearing from the blood vessels in the same timeframe (Figure 5). This suggests that Fe_4A_6 benefits from an enhanced permeability and retention effect which is likely a result from binding interactions with blood pool proteins and a relatively large size compared to small chelate contrast agents.

CONCLUSIONS

Significant T_1 water proton relaxation enhancements were observed in-vitro and in-vivo by linking together four high spin Fe(III) centers in a MOP. Fe_4A_6 has a significantly elevated relaxivity at 8.7 ± 0.3 $mM^{-1}s^{-1}$ per molecule or 2.2 ± 0.1 $mM^{-1}s^{-1}$ per iron (4.7 T at 37 °C) which is attributed in part to having four rigidly connected paramagnetic centers contributing to the relaxation of water protons. The highly symmetric complex Fe_4A_6 has a closed coordination sphere as studied by using single crystal XRD and EPR spectroscopy as well as in solution through variable temperature ^{17}O NMR experiments. This suggests inner-sphere water exchange directly to the paramagnetic centers does not contribute to the observed relaxivity enhancements, instead favoring second- and outer-sphere interactions. This is further supported by EPR spectroscopy in which Fe_4A_6 displays similar spectral features to Fe(III) tris-catecholate complexes with the direct coordination sphere occupied by the catechol donors. DOSY NMR experiments with the Ga(III) analog support a hydrodynamic radius which is consistent with the MOPS behaving as isolated species in solution.

Binding interactions with HSA increased the observed relaxivity of Fe_4A_6 in vitro nearly three-fold at 4.7 T. This change is attributed to increased rotational correlation times upon binding the large globular protein. It was determined through titration experiments that up to five molecules of Fe_4A_6 are bound to protein. These binding interactions are relatively strong and may form a final adduct size of over 80 kDa.

The binding interaction of blood pool proteins is reflected in the bio-distribution and clearance pathway for the self-assembled molecule.[63-64] Significant signal enhancements are observed in the vascular system in BALB/c mice over the course of four hours for Fe_4A_6. The complex had no significant clearance through the renal system observed in traditional chelates like Fe(TOB) and Gd(DOTA) instead clearing through the hepatobiliary system. Notably, the contrast enhancement observed in the bladder for Gd-Albumin is consistent with the presence of free Gd(III) given that serum albumin does not exhibit significant renal clearance.[62] Moreover, the previous study showing renal clearance of iron MOPS[42] is most likely due to the presence of iron oxide impurities as supported by their report of large-sized aggregated particles.

Fe_4A_6 has shown promising tumor enhancement properties in subcutaneous ovarian tumor models. Tumor enhancement is attributed to the enhanced permeability and retention affect for the large protein adduct. Similar uptake and retention was observed for Gd-albumin contrast in ovarian tumors with comparable signal enhancements compared to Fe_4A_6. This work highlights the promise of Fe(III) MOPs as MRI contrast agents given their high r_1 relaxivity, large degree of kinetic inertness and interesting protein binding properties.

ASSOCIATED CONTENT

Supporting Information. "This material is available free of charge via the Internet at http://pubs.acs.org." Spectroscopic methods, synthesis and characterization of complexes, studies of kinetic inertness, relaxivity plots and binding isotherms.

AUTHOR INFORMATION

Corresponding Authors

Janet R Morrow – Department of Chemistry, University at Buffalo, the State University of New York, Buffalo, NY 14260
orchid.org/0000-0003-4160-7688
Email: jmorrow@buffalo.edu

Timothy R. Cook - Department of Chemistry, University at Buffalo, the State University of New York, Buffalo, NY 14260
https://orcid.org/0000-0002-7668-8089
Email: trcook@buffalo.edu

Authors

Gregory E. Sokolow – Department of Chemistry, University at Buffalo, the State University of New York, Buffalo, NY 14260
orcid.org/0000-0002-3997-027X

Matthew R. Crawley – Department of Chemistry, University at Buffalo, the State University of New York, Buffalo, NY 14260
orcid.org/0000-0002-2555- 9543

Daniel R. Morphet – Department of Chemistry, University at Buffalo, the State University of New York, Buffalo, NY 14260
orcid.org/0000-0002-4179-632X

Didar Asik – Department of Chemistry, University at Buffalo, the State University of New York, Buffalo, NY 14260
orchid.org/0000-0001-6924-3770

Joseph A. Spernyak – Department of Cell Stress Biology, Roswell Park Comprehensive Cancer Center, Buffalo, New York, 14263
orchid.org/0000-0002-5049-4737

J. Robert McGray – Department of Immunology, Roswell Park Comprehensive Cancer Center, Buffalo, New York, 14263
orchid.org/0000-0002-7145-8444

Author Contributions

The manuscript was written through contributions of all authors. All authors have given approval to the final version of the manuscript.

Notes

JRM is a co-founder of Ferric Contrast, Inc, a company involved in the development of iron-based contrast agents.

ACKNOWLEDGMENT

J.R.M. and T.R.C. acknowledge the NIH (R21CA256602) and the New York State Center of Excellence for Materials Informatics for support. J.A.S. is partially supported by Roswell Park's NIH P30 grant (CA016056). The authors would like to thank the Chemistry Instrument Center, and Magnetic Resonance Center at the University at Buffalo. This work utilized ICP-MS and FTMS that was purchased with funding from a NSF Major Research Instrumentation Program (NSF CHE-0959565) and National Institutes of Health and the Bruker 500 MHz NMR (NSF CHE-2018160). The authors would like to thank SUNY Fredonia and Dr. Allan J. Cardenas for the use of their X-ray diffractometer

ABBREVIATIONS

MOP, Metal organic polyhedron; MRI, Magnetic resonance imaging; HSA, Human serum albumin; EDA, Ethylenediaminetetraacetic acid; DTPA,Diethylenetriamine pentaacetic acid; NMR, Nuclear magnetic resonance; EPR, Electron paramagnetic resonance; LMCT, Ligand to metal charge transfer; CDTA, (1,2-Cyclohexylenedinitrilo)tetraacetic acid; DOTA, 2,2′,2″,2‴-(1,4,7,10-Tetraazacyclododecane-1,4,7,10-tetrayl)tetraacetic acid;

REFERENCES

1. Haley, T. J.; Raymond, K.; Komesu, N.; Upham, H. C., Toxicological and pharmacological effects of gadolinium and samarium chlorides. *Br. J. Pharmacol. Chemother.* **1961,** *17* (3), 526-532.
2. Rogosnitzky, M.; Branch, S., Gadolinium-based contrast agent toxicity: a review of known and proposed mechanisms. *BioMetals* **2016,** *29* (3), 365-376.
3. Weinmann, H. J.; Brasch, R. C.; Press, W. R.; Wesbey, G. E., Characteristics of gadolinium-DTPA complex: a potential NMR contrast agent. *Am. J. Roentgenol.* **1984,** *142* (3), 619-624.
4. Lauffer, R. B.; Parmelee, D. J.; Dunham, S. U.; Ouellet, H. S.; Dolan, R. P.; Witte, S.; McMurry, T. J.; Walovitch, R. C., MS-325: albumin-targeted contrast agent for MR angiography. *Radiology* **1998,** *207* (2), 529-538.
5. Parmelee, D. J.; Walovitch, R. C.; Ouellet, H. S.; Lauffer, R. B., Preclinical Evaluation of the Pharmacokinetics, Biodistribution, and Elimination of MS-325, a Blood Pool Agent for Magnetic Resonance Imaging. *Invest. Radiol.* **1997,** *32* (12), 741-747.
6. Caravan, P.; Cloutier, N. J.; Greenfield, M. T.; McDermid, S. A.; Dunham, S. U.; Bulte, J. W. M.; Amedio, J. C.; Looby, R. J.; Supkowski, R. M.; Horrocks, W. D.; McMurry, T. J.; Lauffer, R. B., The Interaction of MS-325 with Human Serum Albumin and Its Effect on Proton Relaxation Rates. *J. Am. Chem. Soc.* **2002,** *124* (12), 3152-3162.
7. Hofmann, B.; Bogdanov Jr., A.; Marecos, E.; Ebert, W.; Semmler, W.; Weissleder, R., Mechanism of gadophrin-2 accumulation in tumor necrosis. *J. Magn. Reson. Imaging* **1999,** *9* (2), 336-341.
8. Caravan, P.; Ellison, J. J.; McMurry, T. J.; Lauffer, R. B., Gadolinium(III) chelates as MRI contrast agents: Structure, dynamics, and applications. *Chem. Rev.* **1999,** *99*, 2293-2352.
9. Marckmann, P.; Skov, L.; Rossen, K.; Dupont, A.; Damholt, M. B.; Heaf, J. G.; Thomsen, H. S., Nephrogenic Systemic Fibrosis: Suspected Causative Role of Gadodiamide Used for Contrast-Enhanced Magnetic Resonance Imaging. *J. Am. Soc. Nephrol.* **2006,** *17* (9), 2359-2362.
10. Murata, N.; Gonzalez-Cuyar, L. F.; Murata, K.; Fligner, C.; Dills, R.; Hippe, D.; Maravilla, K. R., Macrocyclic and Other Non–Group 1 Gadolinium Contrast Agents Deposit Low Levels of Gadolinium in Brain and Bone Tissue: Preliminary Results From 9 Patients With Normal Renal Function. *Invest. Radiol.* **2016,** *51* (7), 447-453.
11. Errante, Y.; Cirimele, V.; Mallio, C. A.; Di Lazzaro, V.; Zobel, B. B.; Quattrocchi, C. C., Progressive Increase of T1 Signal Intensity of the Dentate Nucleus on Unenhanced Magnetic Resonance Images Is Associated With Cumulative Doses of Intravenously Administered Gadodiamide in Patients With Normal Renal Function,

Suggesting Dechelation. *Invest. Radiol.* **2014,** *49* (10), 685-690.
12. Miller, J. H.; Hu, H. H.; Pokorney, A.; Cornejo, P.; Towbin, R., MRI Brain Signal Intensity Changes of a Child During the Course of 35 Gadolinium Contrast Examinations. *Pediatrics* **2015,** *136* (6), e1637-e1640.
13. Bruce, R.; Wentland, A. L.; Haemel, A. K.; Garrett, R. W.; Sadowski, D. R.; Djamali, A.; Sadowski, E. A., Incidence of Nephrogenic Systemic Fibrosis Using Gadobenate Dimeglumine in 1423 Patients With Renal Insufficiency Compared With Gadodiamide. *Invest. Radiol.* **2016,** *51* (11).
14. Ranga, A.; Agarwal, Y.; Garg, K. J., Gadolinium based contrast agents in current practice: Risks of accumulation and toxicity in patients with normal renal function. *Indian J. Radiol. Imaging* **2017,** *27* (2), 141-147.
15. Gupta, A.; Caravan, P.; Price, W. S.; Platas-Iglesias, C.; Gale, E. M., Applications for Transition-Metal Chemistry in Contrast-Enhanced Magnetic Resonance Imaging. *Inorg. Chem.* **2020,** *59* (10), 6648-6678.
16. Kuźnik, N.; Wyskocka, M., Iron(III) Contrast Agent Candidates for MRI: a Survey of the Structure–Effect Relationship in the Last 15 -Years of Studies. *Eur. J. Inorg. Chem.* **2016,** *2016* (4), 445-458.
17. Botta, M.; Carniato, F.; Esteban-Gómez, D.; Platas-Iglesias, C.; Tei, L., Mn(II) compounds as an alternative to Gd-based MRI probes. *Future Med. Chem.* **2019,** *11* (12), 1461-1483.
18. Wahsner, J.; Gale, E. M.; Rodríguez-Rodríguez, A.; Caravan, P., Chemistry of MRI Contrast Agents: Current Challenges and New Frontiers. *Chem. Rev.* **2019,** *119* (2), 957-1057.
19. Boehm-Sturm, P.; Haeckel, A.; Hauptmann, R.; Mueller, S.; Kuhl, C. K.; Schellenberger, E. A., Low-Molecular-Weight Iron Chelates May Be an Alternative to Gadolinium-based Contrast Agents for T1-weighted Contrast-enhanced MR Imaging. *Radiology* **2018,** *286* (2), 537-546.
20. Wang, H.; Jordan, V. C.; Ramsay, I. A.; Sojoodi, M.; Fuchs, B. C.; Tanabe, K. K.; Caravan, P.; Gale, E. M., Molecular Magnetic Resonance Imaging Using a Redox-Active Iron Complex. *J. Am. Chem. Soc.* **2019,** *141* (14), 5916-5925.
21. Bales, B. C.; Grimmond, B.; Johnson, B. F.; Luttrell, M. T.; Meyer, D. E.; Polyanskaya, T.; Rishel, M. J.; Roberts, J., Fe-HBED Analogs: A Promising Class of Iron-Chelate Contrast Agents for Magnetic Resonance Imaging. *Contrast Media Mol. Imaging* **2019,** *2019*, 8356931.
22. Wang, H.; Wong, A.; Lewis, L. C.; Nemeth, G. R.; Jordan, V. C.; Bacon, J. W.; Caravan, P.; Shafaat, H. S.; Gale, E. M., Rational Ligand Design Enables pH Control over Aqueous Iron Magnetostructural Dynamics and Relaxometric Properties. *Inorg. Chem.* **2020,** *59* (23), 17712-17721.
23. Snyder, E. M.; Asik, D.; Abozeid, S. M.; Burgio, A.; Bateman, G.; Turowski, S. G.; Spernyak, J. A.; Morrow, J. R., A Class of FeIII Macrocyclic Complexes with Alcohol Donor Groups as Effective T1 MRI Contrast Agents. *Angew. Chemie. Int. Ed.* **2020,** *59* (6), 2414-2419.
24. Asik, D.; Smolinski, R.; Abozeid, S. M.; Mitchell, T. B.; Turowski, S. G.; Spernyak, J. A.; Morrow, J. R., Modulating the Properties of Fe(III) Macrocyclic MRI Contrast Agents by Appending Sulfonate or Hydroxyl Groups. *Molecules* **2020,** *25* (10), 2291.
25. Asik, D.; Abozeid, S. M.; Turowski, S. G.; Spernyak, J. A.; Morrow, J. R., Dinuclear Fe(III) Hydroxypropyl-Appended Macrocyclic Complexes as MRI Probes. *Inorg. Chem.* **2021,** *60* (12), 8651-8664.
26. Palagi, L.; Di Gregorio, E.; Costanzo, D.; Stefania, R.; Cavallotti, C.; Capozza, M.; Aime, S.; Gianolio, E., Fe(deferasirox)2: An Iron(III)-Based Magnetic Resonance Imaging T1 Contrast Agent Endowed with Remarkable Molecular and Functional Characteristics. *J. Am. Chem. Soc.* **2021,** *143* (35), 14178-14188.
27. Davies, J. A.; Dutremez, S. G.; Hockensmith, C. M.; Keck, R.; Richardson, N.; Selman, S.; Smith, D. A.; Ulmer, C. W.; Wheatley, L. S.; Zeiss, J., Iron-based second-sphere contrast agents for magnetic resonance imaging: Development of a model system and evaluation of iron (III) tris (tironate) complex in rats. *Acad. Radiol.* **1996,** *3* (11), 936-945.
28. Maheshwaran, D.; Nagendraraj, T.; Sekar Balaji, T.; Kumaresan, G.; Senthil Kumaran, S.; Mayilmurugan, R., Smart dual T1 MRI-optical imaging agent based on a rhodamine appended Fe(iii)-catecholate complex. *Dalton Trans.* **2020,** *49* (41), 14680-14689.
29. Maheshwaran, D.; Nagendraraj, T.; Sekar Balaji, T.; Kumaresan, G.; Senthil Kumaran, S.; Mayilmurugan, R., Smart dual T(1) MRI-optical imaging agent based on a rhodamine appended Fe(III)-catecholate complex. *Dalton transactions (Cambridge, England : 2003)* **2020,** *49* (41), 14680-14689.
30. Schwert, D. D.; Richardson, N.; Ji, G.; Radüchel, B.; Ebert, W.; Heffner, P. E.; Keck, R.; Davies, J. A., Synthesis of Two 3,5-Disubstituted Sulfonamide Catechol Ligands and Evaluation of Their Iron(III) Complexes for Use as MRI Contrast Agents. *J. Med. Chem.* **2005,** *48* (23), 7482-7485.
31. Li, Y.; Xie, Y.; Wang, Z.; Zang, N.; Carniato, F.; Huang, Y.; Andolina, C. M.; Parent, L. R.; Ditri, T. B.; Walter, E. D.; Botta, M.; Rinehart, J. D.; Gianneschi, N. C., Structure and Function of Iron-Loaded Synthetic Melanin. *ACS Nano* **2016,** *10* (11), 10186-10194.
32. Baranyai, Z.; Carniato, F.; Nucera, A.; Horváth, D.; Tei, L.; Platas-Iglesias, C.; Botta, M., Defining the conditions for the development of the emerging class of FeIII-based MRI contrast agents. *Chem. Sci.* **2021**.
33. Caravan, P.; Ellison, J. J.; McMurry, T. J.; Lauffer, R. B., Gadolinium(III) Chelates as MRI Contrast Agents: Structure, Dynamics, and Applications. *Chem. Rev.* **1999,** *99* (9), 2293-2352.
34. Leone, L.; Ferrauto, G.; Cossi, M.; Botta, M.; Tei, L., Optimizing the Relaxivity of MRI Probes at High Magnetic Field Strengths With Binuclear GdIII Complexes. *Front. Chem.* **2018,** *6* (158).
35. Caravan, P.; Farrar, C. T.; Frullano, L.; Uppal, R., Influence of molecular parameters and increasing magnetic field strength on relaxivity of gadolinium- and manganese-

based T1 contrast agents. *Contrast Media Mol. Imaging* **2009,** *4* (2), 89-100.
36. Major, J. L.; Meade, T. J., Bioresponsive, Cell-Penetrating, and Multimeric MR Contrast Agents. *Acc. Chem. Res.* **2009,** *42* (7), 893-903.
37. Xie, J.; Haeckel, A.; Hauptmann, R.; Ray, I. P.; Limberg, C.; Kulak, N.; Hamm, B.; Schellenberger, E., Iron(III)-tCDTA derivatives as MRI contrast agents: Increased T(1) relaxivities at higher magnetic field strength and pH sensing. *Magn. Reson. Med.* **2021,** *85* (6), 3370-3382.
38. Raymond, K. N.; Pierre, V. C., Next Generation, High Relaxivity Gadolinium MRI Agents. *Bioconjugate Chem.* **2005,** *16* (1), 3-8.
39. Werner, E. J.; Datta, A.; Jocher, C. J.; Raymond, K. N., High-relaxivity MRI contrast agents: where coordination chemistry meets medical imaging. *Angew. Chem. Int. Ed. Engl.* **2008,** *47* (45), 8568-80.
40. Pierre, V. C.; Botta, M.; Aime, S.; Raymond, K. N., Fe(III)-templated Gd(III) self-assemblies-a new route toward macromolecular MRI contrast agents. *J. Am. Chem. Soc.* **2006,** *128* (29), 9272-9273.
41. Morrow, J. R.; Cook, T. R.; Sokolow, G. E.; Rivera, A. Iron(iii) and gallium(iii) metal organic polyhedra, methods of making same, and uses thereof. WO2020263761A1, 2020.
42. Wang, R.; An, L.; He, J.; Li, M.; Jiao, J.; Yang, S., A class of water-soluble Fe(iii) coordination complexes as T1-weighted MRI contrast agents. *J. Mater. Chem. B.* **2021,** *9* (7), 1787-1791.
43. Parac, T. N.; Caulder, D. L.; Raymond, K. N., Selective Encapsulation of Aqueous Cationic Guests into a Supramolecular Tetrahedral [M4L6]12- Anionic Host. *J. Am. Chem. Soc.* **1998,** *120* (31), 8003-8004.
44. Davis, A. V.; Raymond, K. N., The Big Squeeze: Guest Exchange in an M4L6 Supramolecular Host. *J. Am. Chem. Soc.* **2005,** *127* (21), 7912-7919.
45. Caulder, D. L.; Brueckner, C.; Powers, R. E.; Koenig, S.; Parac, T. N.; Leary, J. A.; Raymond, K. N., Design, Formation and Properties of Tetrahedral M4L4 and M4L6 Supramolecular Clusters. *J. Am. Chem. Soc.* **2001,** *123* (37), 8923-8938.
46. Perry, H. L.; Yoon, I. C.; Chabloz, N. G.; Molisso, S.; Stasiuk, G. J.; Botnar, R. M.; Wilton-Ely, J., Metallostar Assemblies Based on Dithiocarbamates for Use as MRI Contrast Agents. *Inorg. Chem.* **2020,** *59* (15), 10813-10823.
47. Livramento, J. B.; Tóth, E.; Sour, A.; Borel, A.; Merbach, A. E.; Ruloff, R., High relaxivity confined to a small molecular space: a metallostar-based, potential MRI contrast agent. *Angew. Chem. Int. Ed. Engl.* **2005,** *44* (10), 1480-4.
48. Evans, D. F., The determination of the paramagnetic susceptibility of substances in solution by nuclear magnetic resonance. *J. Chem. Soc.* **1959**, 2003-5.
49. Megyes, T.; Jude, H.; Grósz, T.; Bakó, I.; Radnai, T.; Tárkányi, G.; Pálinkás, G.; Stang, P. J., X-ray Diffraction and DOSY NMR Characterization of Self-Assembled Supramolecular Metallocyclic Species in Solution. *J. Am. Chem. Soc.* **2005,** *127* (30), 10731-10738.
50. McCarney, E. R.; Breaux, C. J.; Rendle, P. M., Measurement of the hydrodynamic radii of PEE-G dendrons by diffusion spectroscopy on a benchtop NMR spectrometer. *Magn. Reson. Chem.* **2020,** *58* (7), 641-647.
51. Drago, R. S., *Physical methods for chemists*. Saunders College Pub.: 1992.
52. Weisser, J. T.; Nilges, M. J.; Sever, M. J.; Wilker, J. J., EPR Investigation and Spectral Simulations of Iron−Catecholate Complexes and Iron−Peptide Models of Marine Adhesive Cross-Links. *Inorg. Chem.* **2006,** *45* (19), 7736-7747.
53. Cox, D. D.; Benkovic, S. J.; Bloom, L. M.; Bradley, F. C.; Nelson, M. J.; Que, L. J.; Wallick, D. E., Catecholate LMCT bands as probes for the active sites of nonheme iron oxygenases. *J. Am. Chem. Soc.* **1988,** *110* (7), 2026-2032.
54. Aasa, R., Powder Line Shapes in the Electron Paramagnetic Resonance Spectra of High-Spin Ferric Complexes. *J. Chem. Phys.* **1970,** *52* (8), 3919-3930.
55. Galpin, J. R.; Tielens, L. G.; Veldink, G. A.; Vliegenthart, J. F.; Boldingh, J., On the interaction of some catechol derivatives with the iron atom of soybean lipoxygenase. *FEBS Lett.* **1976,** *69* (1), 179-82.
56. Chiou, Y.-M.; Que, L., Structure of a Mononuclear Iron(II)-Catecholate Complex and Its Relevance to the Extradiol-Cleaving Catechol Dioxygenases. *Inorg. Chem.* **1995,** *34* (14), 3577-3578.
57. Bond, C. J.; Sokolow, G. E.; Crawley, M. R.; Burns, P. J.; Cox, J. M.; Mayilmurugan, R.; Morrow, J. R., Exploring Inner-Sphere Water Interactions of Fe(II) and Co(II) Complexes of 12-Membered Macrocycles To Develop CEST MRI Probes. *Inorg. Chem.* **2019,** *58* (13), 8710-8719.
58. Gale, E. M.; Zhu, J.; Caravan, P., Direct Measurement of the Mn(II) Hydration State in Metal Complexes and Metalloproteins through 17O NMR Line Widths. *J. Am. Chem. Soc.* **2013,** *135* (49), 18600-18608.
59. Caravan, P., Protein-Targeted Gadolinium-Based Magnetic Resonance Imaging (MRI) Contrast Agents: Design and Mechanism of Action. *Acc. Chem. Res.* **2009,** *42* (7), 851-862.
60. Longo, D. L.; Arena, F.; Consolino, L.; Minazzi, P.; Geninatti-Crich, S.; Giovenzana, G. B.; Aime, S., Gd-AAZTA-MADEC, an improved blood pool agent for DCE-MRI studies on mice on 1 T scanners. *Biomaterials* **2016,** *75*, 47-57.
61. Ogan, M. D.; Schmiedl, U.; Moseley, M. E.; Grodd, W.; Paajanen, H.; Brasch, R. C., Albumin labeled with Gd-DTPA. An intravascular contrast-enhancing agent for magnetic resonance blood pool imaging: preparation and characterization. *Invest. Radiol.* **1987,** *22* (8), 665-671.
62. Gburek, J.; Konopska, B.; Gołąb, K., Renal Handling of Albumin-From Early Findings to Current Concepts. *Int. J. Mol. Sci.* **2021,** *22* (11), 5809.
63. La Cava, F.; Fringuello Mingo, A.; Miragoli, L.; Terreno, E.; Cappelletti, E.; Lattuada, L.; Poggi, L.; Colombo Serra, S., Synthesis, Characterization, and Biodistribution of a Dinuclear Gadolinium Complex with Improved Properties as a Blood Pool MRI Agent. *ChemMedChem* **2018,** *13* (8), 824-834.

64. Brandt, M.; Cardinale, J.; Giammei, C.; Guarrochena, X.; Happl, B.; Jouini, N.; Mindt, T. L., Mini-review: Targeted radiopharmaceuticals incorporating reversible, low molecular weight albumin binders. *Nucl. Med. Biol.* **2019,** *70*, 46-52.

TEXT (Word Style "TA_Main_Text"). For full instructions, please see the journal's Instructions for Authors. Do not modify the font in this or any other section, as doing so will not give an accurate estimate of the formatting for publication and final length of the paper.

FIGURES (Word Style "VA_Figure_Caption"). Each figure must have a caption that includes the figure number and a brief description, preferably one or two sentences. The caption should follow the format "Figure 1. Figure caption." All figures must be mentioned in the text consecutively and numbered with Arabic numerals. The caption should be understandable without reference to the text. Whenever possible, place the key to symbols in the artwork, not in the caption. To insert the figure into the template, be sure it is already sized appropriately and paste before the figure caption. For formatting double-column figures, see the instructions at the end of the template. Do NOT modify the amount of space before and after the caption as this allows for the rules, space above and below the rules, and space above and below the figure to be inserted upon editing.

SCHEMES (Word Style "VC_Scheme_Title"). Groups of reactions that show action are called schemes. Schemes may have brief titles describing their contents. The title should follow the format "Scheme 1. Scheme Title". Schemes may also have footnotes (use Word Style "FD_Scheme_Footnote"). To insert the scheme into the template, be sure it is already sized appropriately and paste after the scheme title. For formatting double-column schemes, see the instructions at the end of the template. Do NOT modify the amount of space before and after the title as this allows for the rules, space above and below the rules, and space above and below the scheme to be inserted upon editing.

CHARTS (Word Style "VB_Chart_Title"). Groups of structures that do not show action are called charts. Charts may have brief titles describing their contents. The title should follow the format "Chart 1. Chart Title". Charts may also have footnotes (use Word Style "FC_Chart_Footnote"). To insert the chart into the template, be sure it is already sized appropriately and paste after the chart title. For formatting double-column charts, see the instructions at the end of the template. Do NOT modify the amount of space before and after the title as this allows for the rules, space above and below the rules, and space above and below the chart to be inserted upon editing.

TABLES. Each table must have a brief (one phrase or sentence) title that describes its contents. The title should follow the format "Table 1. Table Title" (Word Style "VD_Table_Title"). The title should be understandable without reference to the text. Put details in footnotes, not in the title (use Word Style "FE_Table_Footnote"). Do NOT modify the amount of space before and after the title as this allows for the space above and below the table to be inserted upon editing.

Use tables (Word Style "TC_Table_Body") when the data cannot be presented clearly as narrative, when many precise numbers must be presented, or when more meaningful interrelationships can be conveyed by the tabular format. **Do not use Word Style "TC_Table_Body" for tables containing artwork**. Tables should supplement, not duplicate, text and figures. Tables should be simple and concise. It is preferable to use the Table Tool in your word-processing package, placing one entry per cell, to generate tables.

Displayed equations can be inserted where desired making sure they are assigned Word Style "Normal". Displayed equations can only be one column wide. If the artwork needs to be two columns wide, it must be relabeled as a figure, chart, or scheme and mentioned as such in the text.

SYNOPSIS TOC (Word Style "SN_Synopsis_TOC"). If you are submitting your paper to a journal that requires a synopsis graphic and/or synopsis paragraph, see the Instructions for Authors on the journal's homepage for a description of what needs to be provided and for the size requirements of the artwork.

To format double-column figures, schemes, charts, and tables, use the following instructions:

Place the insertion point where you want to change the number of columns
From the **Insert** menu, choose **Break**
Under **Sections**, choose **Continuous**
Make sure the insertion point is in the new section. From the **Format** menu, choose **Columns**
In the **Number of Columns** box, type **1**
Choose the **OK** button

Now your page is set up so that figures, schemes, charts, and tables can span two columns. These must appear at the top of the page. Be sure to add another section break after the table and change it back to two columns with a spacing of 0.33 in.

Table 1. Example of a Double-Column Table

Column 1	Column 2	Column 3	Column 4	Column 5	Column 6	Column 7	Column 8

Authors are required to submit a graphic entry for the Table of Contents (TOC) that, in conjunction with the manuscript title, should give the reader a representative idea of one of the following: A key structure, reaction, equation, concept, or theorem, etc., that is discussed in the manuscript. Consult the journal's Instructions for Authors for TOC graphic specifications.

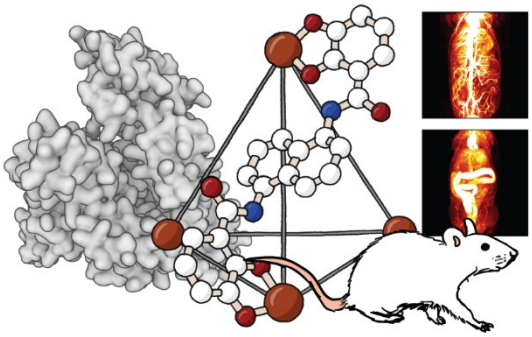

Synopsis: A metal organic polyhedron containing four Fe(III) centers connected with rigid catecholate linkers acts as an effective T_1 MRI contrast agent. Bio-distribution and T_1 relaxivity enhancements are closely tied to albumin binding with long residence times in the vascular system of BALB/c mice and a three-fold enhancement in relaxivity upon binding to serum albumin. Blood protein binding likely contributes to contrast enhancement that is observed in ovarian tumor models up to 24 hours post-injection.